New analytical solutions for weakly compressible Newtonian Poiseuille flows with pressure-dependent viscosity

Kostas D. Housiadas [a,*], Georgios C. Georgiou [b]

[a] Department of Mathematics, University of the Aegean, Karlovassi, 83200 Samos, Greece
[b] Department of Mathematics and Statistics, University of Cyprus, P.O. Box 20537, 1678 Nicosia, Cyprus

ARTICLE INFO

ABSTRACT

Steady-state, isothermal, Poiseuille flows in straight channels and circular tubes of weakly compressible Newtonian fluids are considered. The major assumption is that both the mass density and the shear viscosity of the fluid vary linearly with pressure. The non-zero velocity components, the pressure, the mass density and viscosity of the fluid are represented over the flow domain as asymptotic expansions in which the dimensionless isothermal compressibility coefficient ε is taken as small parameter. A perturbation analysis is performed and asymptotic solutions for all variables are obtained up to first order in ε. The derived solutions, which hold for not necessarily small values of the dimensionless pressure-dependence coefficient, extend previous regular perturbation results and analytical works in the literature for weakly compressible fluids with constant viscosity (solved with a regular perturbation scheme), for incompressible flows with pressure-dependent viscosity (solved analytically), as well as for compressible fluids with pressure-dependent viscosity (solved with double regular perturbation schemes). In contrast to the previous analytical studies in the literature, a non-zero wall-normal velocity is predicted at first order in ε, even at zero Reynolds number. A severe reduction of the volumetric flow-rate at the entrance of the tube/channel and multiplicity of solutions in the flow curves (volumetric flow-rate versus pressure drop) are also predicted. Last, it is shown that weak compressibility of the fluid and the viscosity pressure-dependence have competing effects on the mean friction factor and the average pressure difference required to drive the flow.

© 2016 Elsevier Ltd. All rights reserved.

1. Introduction

The density and the viscosity of a fluid depend on both the temperature and the pressure. In certain cases, the dependence of the viscosity on pressure may be much stronger than that of the density, e.g., with polymer melts (Denn, 2008; Renardy, 2003) and lubricants (Rajagopal, 2006; Rajagopal, Saccomandi, & Vergori, 2012). This dependence becomes important in many applications involving high pressures or a large pressure range, such as polymer and food processing (Dealy & Wang, 2013), crude oil and fuel oil pumping (Martinez-Boza, Martin-Alfonso, Callegos, & Fernández, 2011; Schaschke, Fletcher, & Glen, 2013), fluid film lubrication (Hamrock, Schmid, & Jaconson, 2004), microfluidics (Silber-Li, Cui, Tan, & Tabeling, 2006), filtration through porous media (Fusi, Farina, & Rosso, 2015), certain geophysical flows (Schoof, 2007; Stemmer, Harder, & Hansen, 2006), and dense flows of dry granular materials (Ionescu, Mangeney, Bouchut, & Roche, 2015). Experimental works

---

* Corresponding author.
  E-mail addresses: housiada@aegean.gr (K.D. Housiadas), georgios@ucy.ac.cy (G.C. Georgiou).

concerning the determination of the pressure-dependence of viscosity using mostly modified capillary rheometers can be found in the recent article by Li, Jiang, Wu, Yuan, and Li (2015).

In order to describe the pressure-dependence of the viscosity a linear law (Barus, 1891, 1893; Renardy, 2003; Georgiou, 2003; Kalogirou, Poyiadji & Georgiou, 2011) is often used:

$$\eta^* = \eta_0^*\left[1 + \beta^*(p^* - p_{ref}^*)\right] \tag{1}$$

where η_* is the shear viscosity, p_* is the pressure, η_0^* is the viscosity at the reference pressure p_{ref}^*, and β_* is a positive parameter often referred to as the viscosity-pressure-dependence coefficient. Throughout the text a superscript star indicates a dimensional quantity; hence symbols without stars are dimensionless. In general, β_* depends on the temperature, the pressure, and the shear rate (Gustafsson, Rajagopal, Stenberg, & Videman, 2015). In isothermal Newtonian flows β_* is usually assumed to be a constant. Its values are in the range of 10–70 GPa^{-1} for lubricants (Kottke, Bair, & Winer, 2003; Tanner, 2000), 10–50 GPa^{-1} for polymer melts (Dealy & Wang, 2013; Denn, 2008; Kadjik & Van Den Brule, 1994; Tanner, 2000), and 10–20 GPa^{-1} for mineral oils (Venner & Lubrecht, 2000). Other expressions (such as the exponential law) resulting to a better fitting of available experimental data on complex fluids at different pressures have been reviewed by Málek and Rajagopal (2007) and by Housiadas (2015). Both Eqs. (1) and (2) have been employed extensively in the literature for a variety of simple flows which are important for both theoretical and experimental purposes; these include the flow due to a suddenly accelerated plate or due to an oscillating plate (Prusa, 2010; Srinivasan & Rajagopal, 2009), as well as well the laminar flows in circular tubes and straight channels (Housiadas 2015; Kalogirou et al., 2011; Poyiadji, Housiadas, Kaouri, & Georgiou, 2015; Renardy, 2003). In all cases, viscosity pressure-dependence has been found to have a substantial effect on the flow field and on features such as the skin friction factor and the pressure difference required to drive the flow.

The mass density of a liquid is expected to change at high pressures, even under isothermal conditions. Hence, the modeling of compressible flows is the subject of many works in the literature, especially in the case of complex fluids. A brief survey, for both Newtonian and viscoelastic Maxwell-type fluids, and in the framework of non-equilibrium thermodynamics, has been presented by Bollada and Phillips (2012). For Newtonian compressible liquids, a linear equation of state relating the mass density of the fluid to the total pressure is very often used (see, e.g., Venerus, 2006).

$$\rho^* = \rho_0^*\left[1 + \varepsilon^*(p^* - p_{ref}^*)\right] \tag{2}$$

where ρ_0^* is the mass density of the fluid at the reference pressure p_{ref}^* and ε_* is the constant isothermal compressibility. Eq. (2) has been used in numerical simulations of weakly compressible liquid flows in long tubes, such as waxy crude oil (Vinay, Wachs, & Frigaard, 2006) and polymer extrusion (Taliadorou, Georgiou, & Mitsoulis, 2008).

Eqs. (1) and (2) introduce nonlinearities into the continuity and momentum equations, even for steady state, isothermal, laminar, creeping flow conditions, thus making the derivation of analytical solutions a very difficult task. Incompressible Newtonian flows with pressure-dependent viscosity have been analyzed mathematically by various investigators (see, e.g., Housiadas, Georgiou, & Tanner, 2015; Huilgol & You, 2006; Rehor & Prusa, 2016; and Vasudevaiah & Rajagopal, 2005; and references therein). Kalogirou et al. (2011) compiled analytical, two-dimensional, solutions for Poiseuille flows in a straight channel, a circular tube, and an annulus with constant inner and outer radius for an incompressible Newtonian fluid ($\varepsilon^* = 0$) obeying the linear Eq.(2) under the above-mentioned conditions. More recently, Housiadas et al. (2015) obtained perturbation solutions of the unbounded creeping flow past a sphere of a Newtonian fluid under the assumption that the shear viscosity varies either linearly or exponentially with pressure, taking the dimensionless pressure-viscosity coefficient as the perturbation parameter.

Analytical and numerical studies for compressible laminar flow of a Newtonian fluid in a tube have been conducted by van den Berg, Seldam, and van der Gulik (1993). Significant corrections to the volumetric flow-rate, compared to the predictions of the classical Poiseuille law have been revealed. The origin of those corrections was the equation of the state, i.e., from the equation that relates the mass density of the fluid to the total pressure. Analytical perturbation solutions for weakly compressible Newtonian fluids in channels and tubes, with the isothermal compressibility coefficient serving as the perturbation parameter, have been derived by Venerus and co-worker (Venerus, 2006; Venerus & Bugajsky, 2010) as well as by Taliadorou, Neophytou, and Georgiou (2009).

However, analytical studies that take into account both the compressibility and the viscosity pressure-dependence are very scarce in the literature. Recently, Poyiadji et al. (2015) derived analytical solutions for steady axisymmetric and planar Poiseuille flows of weakly compressible isothermal Newtonian liquids, using Eqs. (1)–(2) and a double regular asymptotic expansion for all the primary flow variables with small parameters the dimensionless pressure-viscosity coefficient, β, and the dimensionless coefficient of compressibility, ε (for their definitions see Section 2). Assuming that $\varepsilon \approx \beta$, they derived solutions up to second order for both parameters and analyzed the combined effects of weak compressibility and the pressure-dependent viscosity.

In the present work, the solution of Poyiadji et al. (2015) is extended by relaxing the assumption of a small β; a regular perturbation scheme is utilized in terms of ε only. By doing so, however, non-linear terms are retained into the governing equations while the solution reveals features of the flow not predicted by the double perturbation analysis. Thus, the analytical solutions derived here are valid for small values of ε and any value of β.

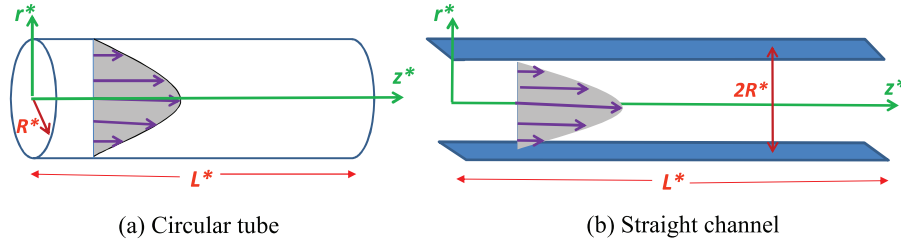(a) Circular tube   (b) Straight channel

Fig. 1. Geometrical flow configurations and coordinate systems: (a) circular tube; (b) straight channel.

2. Problem formulation

The steady, weakly compressible isothermal flow of a Newtonian fluid with pressure-dependent viscosity, and no external forces or torques, is considered. Two flows are studied the geometries of which are sketched in Fig. 1: (a) the axisymmetric Poiseuille flow in a circular tube of constant radius R_* and length L_* in cylindrical coordinates (r_*, z_*); (b) the planar Poiseuille flow in a straight channel (or slit) of height $2R_*$ and length L_* in Cartesian coordinates (z_*, r_*) centered at the midplane. Thus, in both cases, z_* is along the main flow direction and r_* is along the transverse direction, perpendicular to the wall. Under these assumptions, the mass and momentum equations can be written as follows:

$$\nabla^* \cdot (\rho^* \mathbf{u}^*) = 0 \tag{3}$$

$$-\nabla^* p^* + \nabla^* \cdot \boldsymbol{\tau}^* = \mathbf{0} \tag{4}$$

where $\mathbf{u}^*$ is the velocity vector, $\boldsymbol{\tau}^*$ is the viscous extra-stress symmetric tensor given by

$$\boldsymbol{\tau}^* = \eta^* \dot{\boldsymbol{\gamma}}^* \tag{5}$$

and $\dot{\boldsymbol{\gamma}}^*$ is the augmented rate-of-deformation tensor:

$$\dot{\boldsymbol{\gamma}}^* = \nabla^* \mathbf{u}^* + (\nabla^* \mathbf{u}^*)^T - \frac{2}{3}\mathbf{I}(\nabla^* \cdot \mathbf{u}^*) \tag{6}$$

The superscript T denotes the transpose, and $\mathbf{I}$ is the unit tensor. The shear viscosity η_* and the mass density ρ_* are assumed to obey Eqs. (1) and (2), respectively.

In order to follow a unified approach for both flow configurations and avoid unnecessary repetitions, an auxiliary parameter ξ is introduced such that $\xi = 1$ for the axisymmetric flow and $\xi = 0$ for the planar configuration. The governing equations are rendered dimensionless scaling r_* by R_*, z_* by L_*, u_z^* by the mean velocity U_* at the tube/channel exit, u_r^* by $U_* R_*/L_*$, and $p^* - p_{ref}^*$ by $(3+5\xi)\eta_0^* L^* U^*/R^{*2}$. The mass density and the viscosity are scaled by ρ_0^* and η_0^*, respectively. Thus, the dimensionless forms of the continuity equation, Eq. (3), the two components of the momentum equation, (Eq. 4), the four non-zero components of the extra stress-tensor $\boldsymbol{\tau}_*$, Eq. (5), the equation of state, Eq. (2), and the equation for the shear viscosity, Eq. (1), become:

$$\frac{\partial (r^\xi \rho u_r)}{\partial r} + \frac{\partial (r^\xi \rho u_z)}{\partial z} = 0 \tag{7}$$

$$-(3+5\xi)\frac{\partial p}{\partial z} + a^2 \frac{\partial \tau_{zz}}{\partial z} + a\left(\frac{\partial \tau_{rz}}{\partial r} + \xi \frac{\tau_{rz}}{r}\right) = 0 \tag{8}$$

$$-(3+5\xi)\frac{\partial p}{\partial r} + a^2\left(a\frac{\partial \tau_{rz}}{\partial z} + \frac{\partial \tau_{rr}}{\partial r} + \xi \frac{\tau_{rr} - \tau_{\theta\theta}}{r}\right) = 0 \tag{9}$$

$$\tau_{zz} = \eta\left[\frac{4}{3}\frac{\partial u_z}{\partial z} - \frac{2}{3}\left(\frac{\partial u_r}{\partial r} + \xi \frac{u_r}{r}\right)\right] \tag{10a}$$

$$\tau_{rz} = \eta\left(a\frac{\partial u_r}{\partial z} + \frac{1}{a}\frac{\partial u_z}{\partial r}\right) \tag{10b}$$

$$\tau_{rr} = \eta\left[\frac{4}{3}\frac{\partial u_r}{\partial r} - \frac{2}{3}\left(\frac{\partial u_z}{\partial z} + \xi \frac{u_r}{r}\right)\right] \tag{10c}$$

$$\tau_{\theta\theta} = \eta\left[\frac{4\xi}{3}\frac{u_r}{r} - \frac{2}{3}\left(\frac{\partial u_r}{\partial r} + \frac{\partial u_z}{\partial z}\right)\right] \tag{10d}$$

$$\rho = 1 + \varepsilon p \tag{11}$$

$$\eta = 1 + \beta p \tag{12}$$

In the above equations three dimensionless numbers appear. The aspect ratio of the tube/channel, a, the dimensionless compressibility number, ε, and the viscosity pressure-dependence number, β, respectively defined by:

$$a \equiv \frac{R^*}{L^*}, \quad \varepsilon \equiv \frac{(3+5\xi)\varepsilon^*\eta_0^*L^*U^*}{R^{*2}}, \quad \beta \equiv \frac{(3+5\xi)\beta^*\eta_0^*L^*U^*}{R^{*2}} \tag{13}$$

The system of Eqs. (7)–(12) closes with appropriate auxiliary conditions. Along the axis of symmetry, symmetry conditions are applied:

$$\frac{\partial u_z}{\partial r}(0, z) = u_r(0, z) = 0, \quad 0 \le z \le 1 \tag{14}$$

Also, no-slip and no-penetration are imposed along the wall(s):

$$u_r(1, z) = u_z(1, z) = 0, \quad 0 \le z \le 1 \tag{15}$$

Moreover, the pressure datum is set at the tube/channel exit,

$$p(1, 1) = 0 \tag{16}$$

and the dimensionless mass flow-rate at the outlet plane is unity:

$$\int_0^1 (2r)^\xi \rho(r, 1) u_z(r, 1) dr = 1 \tag{17}$$

3. Solution

Under the assumption that the compressibility number ε is small, the primary flow variables can be expressed as asymptotic power series in ε:

$$X = X_0 + \varepsilon X_1 + \varepsilon^2 X_2 + O(\varepsilon^3) \tag{18}$$

where $X \in \{p, u_r, u_z, \rho, \eta, \tau_{rr}, \tau_{rz}, \tau_{zz}, \tau_{\theta\theta}\}$. Substituting the above expansions into the governing equations and collecting terms of the same order, a sequence of systems of partial differential equations at each order $O(\varepsilon^j), j = 0, 1, 2, \ldots$ is derived along with the corresponding boundary conditions. The zero-order equations have been solved analytically for all the primary flow variables and for both planar and axisymmetric configurations (Kalogirou et al., 2011). The velocity profile is unidirectional ($u_{r0} = 0, u_{z0} \neq 0$) and depends only on the wall-normal coordinate, while the pressure, the shear viscosity, and the extra-stress components are two-dimensional. The solution can be written concisely as follows:

$$u_{z0}(r) = -\frac{3+5\xi}{(\alpha\beta)^2\lambda} \ln(\hat{p}_0(r)) \tag{19}$$

$$p_0(r, z) = \frac{1}{\beta}\left(\hat{p}_0(r)e^{\lambda\beta(1-z)} - 1\right) \tag{20}$$

$$\eta_0(r, z) = \hat{p}_0(r)e^{\lambda\beta(1-z)} \tag{21}$$

In the above expressions $\hat{p}_0$ is given by

$$\hat{p}_0(r) = \begin{cases} \dfrac{I_0(\alpha\beta\lambda r)}{I_0(\alpha\beta\lambda)}, & \text{axisymmetric} \\[4mm] \dfrac{\cosh(\alpha\beta\lambda r)}{\cosh(\alpha\beta\lambda)}, & \text{planar} \end{cases} \tag{22}$$

where I_0 is the modified Bessel function of zero order, and λ is the root of

$$\int_0^1 (2r)^\xi \ln(\hat{p}_0(r)) dr = -\frac{(\alpha\beta)^2\lambda}{3+5\xi} \tag{23}$$

Eq. (23) results from Eq. (17) at zero order. It cannot be solved analytically; however, it is straightforward to obtain the following asymptotic solutions:

$$\lambda_{as} = \begin{cases} 1 + \dfrac{B^2}{12} + \dfrac{B^4}{96} + \dfrac{11B^6}{7680} + \dfrac{169B^8}{829440} + O(B^{10}), & \text{axisymmetric} \\[4mm] 1 + \dfrac{B^2}{5} + \dfrac{11B^4}{175} + \dfrac{533B^6}{23625} + \dfrac{5231B^8}{606375} + O(B^{10}), & \text{planar} \end{cases} \tag{24}$$
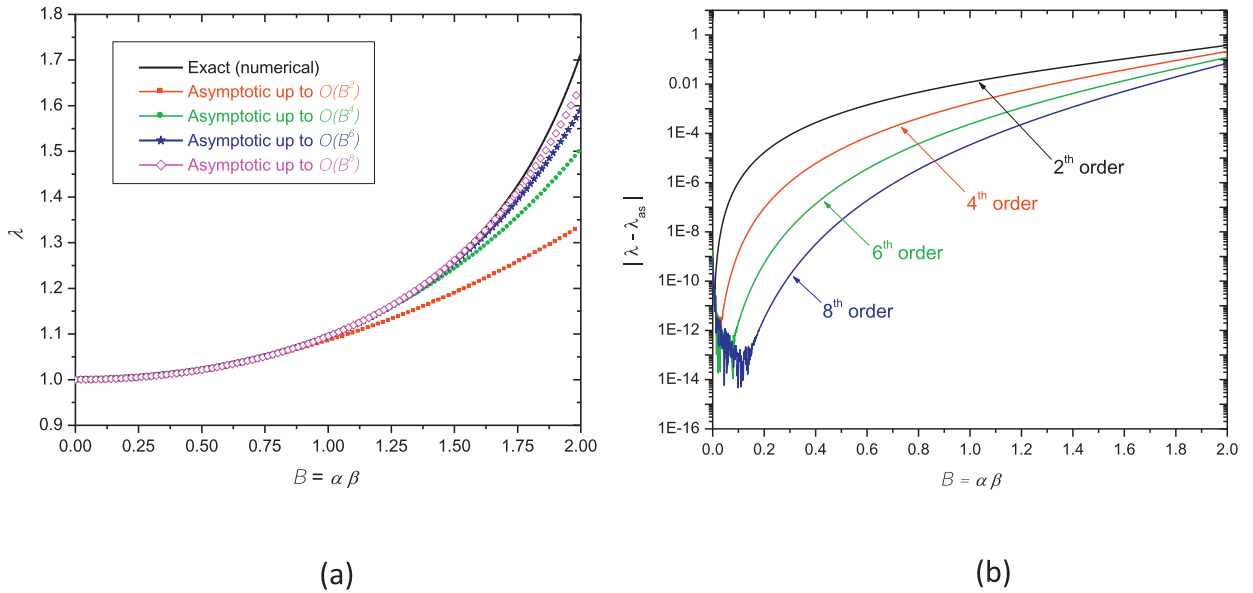
(a)   (b)

Fig. 2. (a) The root of Eq. (23) in the axisymmetric flow as a function of the modified pressure-viscosity coefficient $B = \alpha \beta$; (b) The absolute error of the asymptotic value of λ predicted by Eq. (24).

where $B \equiv \alpha \beta$ is a modified dimensionless pressure-viscosity coefficient. In Fig. 2a the exact solution for λ in the case of axisymmetric flow calculated numerically solving Eq. (23) is compared with the asymptotic solutions calculated from Eq. (24) up to $O(B^k)$, $k = 2, 4, 6, 8$. Clearly, the asymptotic expression up to $O(B^8)$ is an excellent representation of the exact solution up to $B = a\beta \approx 1.8$, which is well-above the range of interest for practical applications. Fig. 2b shows the absolute errors $|\lambda - \lambda_{as}|$ versus B; as the order of approximation increases the absolute error drops, indicating the accuracy and consistency of λ_{as}. Thus, the parameter λ can be calculated either from Eq. (23) or from Eq. (24) since in the range of ε and β for which the perturbation solution is valid, the difference between the exact and the asymptotic expressions is negligible.

The equations at first order in ε have been solved and the complete solutions for all the primary flow variables up to $O(\varepsilon)$ are given below. Whenever quantities that cannot be calculated analytically appear, high-order asymptotic expressions are provided; these expressions are excellent approximations of the corresponding exact quantities up to $B \equiv \alpha \beta \approx 1$.

3.1. Axisymmetric flow

In the axisymmetric case ($\xi = 1$)the solutions for $u_r = u_r(r, z)$, $p = p(r, z)$ and $u_z = u_z(r, z)$ are:

$$u_r \approx \varepsilon \hat{u}_{r1} e^{\lambda \beta (1-z)} \tag{25}$$

$$p \approx \frac{\hat{p}_0 e^{\lambda \beta (1-z)} - 1}{\beta} + \varepsilon \hat{p}_0 e^{\lambda \beta (1-z)} \left\{ \frac{(1-z)/\beta - a^2 \lambda (1 - r^2)/2 + a^2 \lambda \, \varphi(r; 1)}{2 - \lambda^{-1} - \varphi(0; 3)} + \hat{p}_0 h e^{\lambda \beta (1-z)} - h(1) \right\} \tag{26}$$

$$u_z \approx -\frac{8 \ln(\hat{p}_0)}{B^2 \lambda} + \varepsilon \left\{ \frac{4 \left[(1 - r^2) - \varphi(r; 1) + \ln(\hat{p}_0^2)/(B\lambda)^2 \right]}{\beta \left(2 - \lambda^{-1} - \varphi(0; 3) \right)} + \frac{e^{\lambda \beta (1-z)}}{\lambda \beta} \left(\frac{\hat{p}_0 \ln(\hat{p}_0^8)}{B^2} + \frac{\hat{u}_{r1}}{r} + \hat{u}_{r1}' \right) \right\} \tag{27}$$

where $\varphi(r; k) := \int_r^1 (2s)^k \frac{I_1^2(a\lambda\beta s)}{I_0^2(a\lambda\beta s)} ds$ has been defined for compactness, $\hat{p}_0$ is given by Eq. (22), and $h = h(r)$ is an auxiliary function given in terms of $\hat{p}_0$ and $\hat{u}_{r1}$. Thus, the solution (25)– (27) is fully determined if $\hat{u}_{r1} = \hat{u}_{r1}(r)$ is known. The ordinary differential equation for $\hat{u}_{r1}$ and the accompanying boundary conditions and auxiliary functions are provided in the Appendix. No analytical solution could be derived for $\hat{u}_{r1}$, however suitable high-order asymptotic expressions for $\hat{u}_{r1}(r)$, $h(r)$, $\varphi(r; 1)$, and $\varphi(0; 3)$ are:

$$\hat{u}_{r1}(r) \approx -\frac{5r^3 (1 - r^2)^2}{36} B^2 \left(1 + \frac{138 - 47r^2}{960} B^2 + \frac{1337 - 1134r^2 + 507r^4}{46080} B^4 \right.$$

$$\left. + \frac{172\,822 - 238\,851r^2 + 17\,3376r^4 - 41\,697r^6}{27\,648\,000} B^6 \right) \tag{28}$$
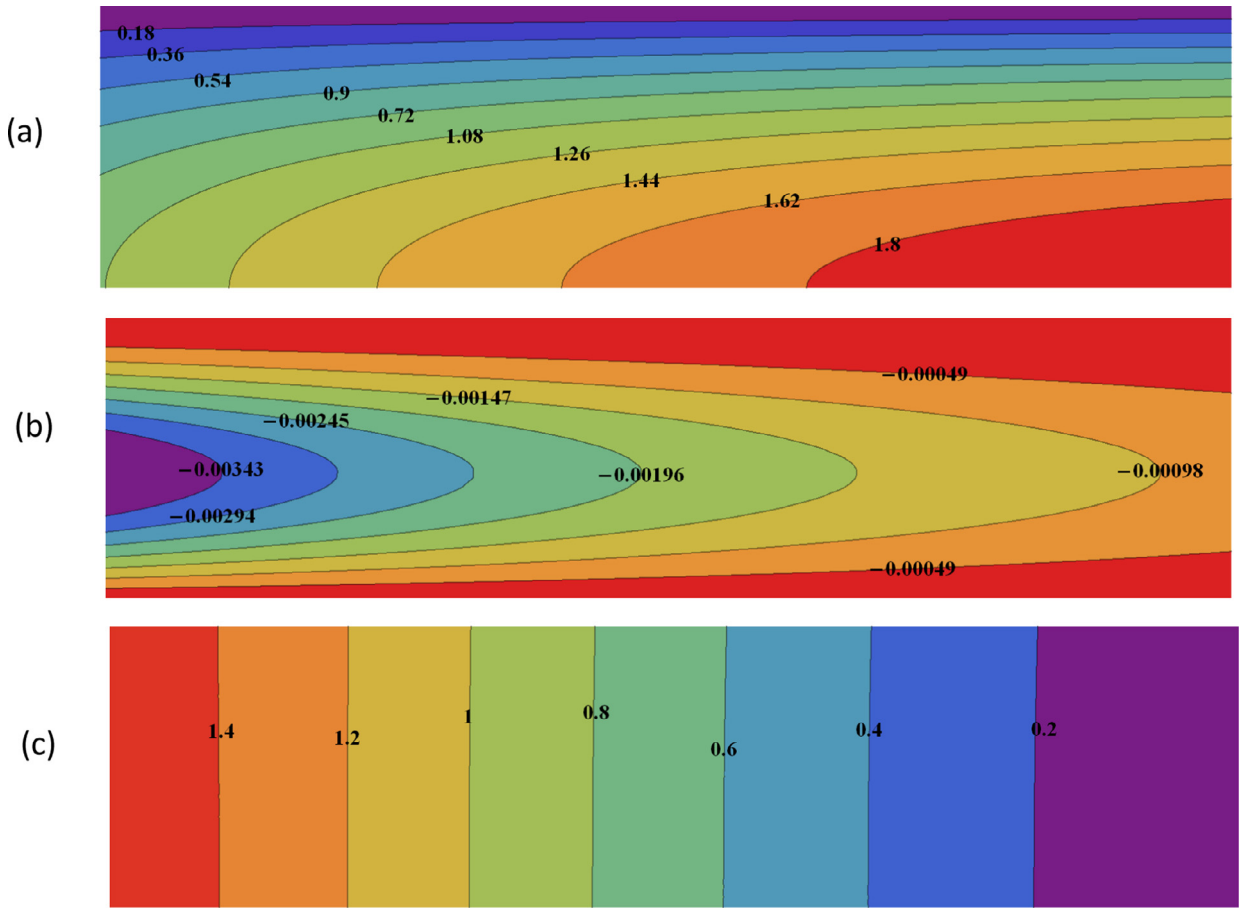
Fig. 3. Contour plots for the axisymmetric flow with $\varepsilon = 0.2$, $\alpha = 0.1$, and $\beta = 1.5$: (a) Axial velocity; (b) Radial velocity; (c) Pressure.

$$h(r) \approx \frac{1}{\beta^2}\left(-1 + \frac{13 - 12r^2}{36}B^2 + \frac{69 - 16r^2}{1152}B^4 + \frac{99 - 166r^2 + 282r^4 - 138r^6}{6912}B^6\right.$$
$$\left. + \frac{71\,453 - 272\,088r^2 + 558\,270r^4 - 444\,000r^6 + 120\,195r^8}{19\,906\,560}B^8\right) \tag{29}$$

$$\varphi(r;1) \approx \frac{(1-r^2)B^2}{8}\left(1 + r^2 - \frac{r^4}{6}B^2 + \frac{1 + r^2 - 31r^4 + 33r^6}{1152}B^4 + \frac{1 + r^2 - 52r^4 + 108r^6 - 57r^8}{11520}B^6\right) \tag{30}$$

$$\varphi(0;3) \approx \frac{B^2}{3}\left(1 - \frac{B^2}{48} - \frac{B^4}{2880} - \frac{B^6}{46080}\right) \tag{31}$$

It is interesting to notice that $\hat{u}_{r1}(r)$, $h(r)\beta^2$, $\varphi(r;1)$ and $\varphi(0;3)$ are functions of the modified pressure-viscosity coefficient $B \equiv a\beta$. These asymptotic expressions also show that the transverse velocity, u_r, is of $O(B^2\varepsilon)$, i.e., much smaller than the first correcting term for the velocity along the main flow direction, u_z, which is of $O(\varepsilon)$.

Contour plots of the axial and radial velocity components and the pressure for a fluid with $\varepsilon = 0.2$, $\beta = 1.5$, and $a = 0.1$ are given in Fig. 3. First, it can be seen that the magnitude of the radial velocity is much smaller that the axial velocity. Also, u_r is larger closer to the entrance of the tube as it should be expected due to the exponential decrease of u_r with the distance from the inlet plane (see Eq. (25)). Consequently, the closer to the entrance the larger the deviation from the simple parabolic profile. Recall that the parabolic profile for an incompressible Newtonian fluid with variable viscosity (i.e., $u_r = 0$ and $u_z = u_z(r)$) corresponds to straight contour lines parallel to the axis of symmetry of the tube. Indeed, Fig. 3b shows that the contours of u_z are significantly curved towards the horizontal axis, indicating that the fluid moves faster close to the axis of symmetry and towards the exit of the tube, and slower close to the entrance and towards the wall. On the other hand, the pressure contours are practically straight lines vertical to the wall; thus the fluid compressibility does not have a significant effect on the variation of the pressure along the radial direction.

3.2. Planar flow

For the planar case ($\xi = 0$) the solution is given by:

$$u_r \approx \varepsilon \hat{u}_{r1} e^{\lambda \beta (1-z)} \tag{32}$$

$$p \approx \frac{\hat{p}_0 e^{\lambda \beta (1-z)} - 1}{\beta} + \varepsilon \hat{p}_0 e^{\lambda \beta (1-z)} \left\{ \frac{\lambda a [1 - z + a(r \tanh(B\lambda r) - \tanh(B\lambda))]}{3 \tanh(B\lambda) - 2B} + \hat{p}_0 h e^{\lambda \beta (1-z)} - h(1) \right\} \tag{33}$$

$$u_z \approx -\frac{3 \ln(\hat{p}_0)}{B^2 \lambda} + \varepsilon \left\{ \frac{3(\tanh(B\lambda) - r \tanh(B\lambda r)) + \ln(\hat{p}_0^3)/(B\lambda)}{\beta (3 \tanh(B\lambda) - 2B)} + \frac{e^{\lambda \beta (1-z)}}{\lambda \beta} \left(\frac{\hat{p}_0 \ln(\hat{p}_0^3)}{B^2} + \hat{u}_{r1}' \right) \right\} \tag{34}$$

where $\hat{p}_0$ is given by Eq. (22) and high-order asymptotic expressions for $\hat{u}_{r1}$ and h are:

$$\hat{u}_{r1}(r) \approx -\frac{11r(1-r^2)^2}{40} B^2 \left(1 + \frac{173 - 85r^2}{770} B^2 + \frac{5793 - 7190r^2 + 3965r^4}{83\,160} B^4 \right.$$
$$\left. + \frac{7\,435\,723 - 16\,839\,665r^2 + 16\,836\,225r^4 - 5\,021\,275r^6}{320\,166\,000} B^6 \right) \tag{35}$$

$$h(r) \approx \frac{1}{\beta^2} \left(-1 + \frac{11 - 10r^2}{15} B^2 + \frac{359 - 126r^2 + 35r^4}{1260} B^4 + \frac{13761 - 17790r^2 + 34125r^4 - 17500r^6}{94500} B^6 \right.$$
$$\left. + \frac{225311 - 614515r^2 + 1492755r^4 - 1324785r^6 + 394350r^8}{3\,118\,500} B^8 \right) \tag{36}$$

As in the axisymmetric case, $\hat{u}_{r1}$ and $h\beta^2$ are functions of B and the wall normal velocity is of $O(B^2 \varepsilon)$. The results for the primary flow variables (axial and transversal velocity components, and the pressure) are very similar to those for the axisymmetric flow in a circular tube (not shown here though).

4. Results and discussion

In this section the analytical solutions are discussed with the emphasis put on quantities relevant to internal pressure-driven flows, i.e., the volumetric flow-rate Q, the average pressure drop required to drive the flow $\Delta \bar{p}$ (where the overbar means averaging in the wall normal direction), and the mean (along the main flow direction) Darcy friction factor $\hat{f}$, which are defined as follows:

$$Q(z) \equiv \int_0^1 (2r)^\xi u_z(r, z) dr \tag{37}$$

$$\Delta \bar{p} \equiv \int_0^1 (2r)^\xi [p(r, z = 0) - p(r, z = 1)] dr \tag{38}$$

$$\hat{f} \equiv \frac{Re}{8(3 + \xi)} \int_0^1 D_f(z) dz = -\frac{a}{3 + \xi} \int_0^1 \tau_{rz}(1, z) dz \tag{39}$$

where D_f is the local Darcy friction factor, and Re is the Reynolds number:

$$D_f(z) \equiv \frac{8|\tau_{rz}^*(R^*, z^*)|}{\rho_0^* U^{*2}}, \quad Re \equiv \frac{\rho_0^* U^* R^*}{\eta_0^*} \tag{40}$$

Alternatively, $\hat{f}$ can be calculated from the momentum equation along the main flow direction, Eq. (8), as follows:

$$\hat{f} = \Delta \bar{p} - \frac{a^2}{3 + 5\xi} \Delta \bar{\tau}_{zz} \tag{41}$$

Here the operator Δ is defined by $\Delta f := f(z = 0) - f(z = 1)$. For incompressible unidirectional Newtonian flow, namely at zero-order in ε, $Q_0(z) = 1$ and $\Delta \bar{\tau}_{zz0} = 0$. Thus, the volumetric flow-rate is constant, and the mean Darcy friction factor simply represents the dimensionless average pressure drop required to drive the flow, i.e., $\hat{f}_0 = \Delta \bar{p}_0$, where

$$\Delta \bar{p}_0 = \begin{cases} \dfrac{2(e^{\lambda \beta} - 1)}{\alpha \beta^2 \lambda} \dfrac{I_1(\alpha \beta \lambda)}{I_0(\alpha \beta \lambda)}, & \text{axisymmetric} \\ \dfrac{(e^{\lambda \beta} - 1)}{\alpha \beta^2 \lambda} \tanh(\alpha \beta \lambda), & \text{planar} \end{cases} \tag{42}$$

As expected, the limit of $\Delta \bar{p}_0$ as β goes to zero is unity.

4.1. Axisymmetric flow

Using the analytical solution at zero- and first-order in ε, one can derive the following expressions:

$$Q(z) = 1 + \frac{\varepsilon}{\beta}\left\{ 1 + \frac{8e^{\lambda\beta(1-z)}q_1}{B^2\lambda} \right\} \tag{43}$$

$$\Delta\bar{p} = \Delta\bar{p}_0 + \varepsilon\left\{ \frac{2(1-e^{\lambda\beta})}{a\lambda\beta}\frac{I_1(B\lambda)}{I_0(B\lambda)}h(1) + (e^{2\lambda\beta}-1)\Phi_1 \right.$$
$$\left. + \frac{1}{(2-\lambda^{-1}-\varphi(0;3))}\left(\frac{2(1-e^{\lambda\beta})}{\lambda\beta^2}\frac{I_2(B\lambda)}{I_0(B\lambda)} + \frac{2e^{\lambda\beta}}{a\lambda\beta^2}\frac{I_1(B\lambda)}{I_0(B\lambda)} + a^2\lambda(e^{\lambda\beta}-1)G_1 \right) \right\} \tag{44}$$

$$\hat{f} = \Delta\bar{p}_0 + \varepsilon\left\{ \frac{2}{\lambda\beta^2(2-\lambda^{-1}-\varphi(0;3))}\left((e^{\lambda\beta}-1)\left(1-\frac{I_1^2(B\lambda)}{I_0^2(B\lambda)}\right) + \frac{2+e^{\lambda\beta}(\lambda\beta-2)}{a\beta\lambda}\frac{I_1(B\lambda)}{I_0(B\lambda)} \right) \right.$$
$$\left. + \frac{1-e^{\lambda\beta}}{\lambda\beta^2}\left[\frac{1+\beta^2h(1)+e^{\beta\lambda}(1-\beta^2h(1))}{B}\frac{I_1(B\lambda)}{I_0(B\lambda)} + \frac{1+e^{\lambda\beta}}{8\lambda}\hat{u}_{r1}''(1) \right] \right\} \tag{45}$$

where I_k is the modified Bessel function of k-order, $h(1)$ is found from Eq. (29) at $r=1$, $\hat{u}_{r1}''(1)$ from Eq. (28), and the quantities Φ_1, G_1, q_1 are defined as follows:

$$\Phi_1 \equiv \int_0^1 2r\hat{p}_0^2(r)h_2(r)dr, \quad G_1 \equiv \int_0^1 2r\left[\left(\int_r^1 \left(\frac{\hat{p}_0'(s)}{\hat{p}_0(s)}\right)^2 ds\right) \right]\hat{p}_0(r)dr, \quad q_1 \equiv \int_0^1 2r\hat{p}_0(r)\ln(\hat{p}_0(r))dr \tag{46}$$

High-order asymptotic expressions for Φ_1, G_1, and q_1 are:

$$\Phi_1 \approx \frac{1}{\beta^2}\left(-1 + \frac{4B^2}{9} - \frac{35B^4}{1152} + \frac{25B^6}{6912} + \frac{89B^8}{1990656} - \frac{6707B^{10}}{26542080} \right)$$
$$G_1 \approx \frac{B^2}{20}\left(1 - \frac{29B^2}{168} + \frac{5B^4}{4032} - \frac{271B^6}{3548160} \right)$$
$$q_1 \approx \frac{B^2}{8}\left(-1 + \frac{B^2}{12} + \frac{B^4}{288} + \frac{B^6}{2880} \right) \tag{47}$$

It is also interesting to report here the limits of equations (43)–(45) as β and ε go to zero. One can find:

$$\lim_{\varepsilon\to 0} Q(z) = 1, \quad \lim_{\beta\to 0} Q(z) = 1 - \varepsilon(1-z)$$
$$\lim_{\varepsilon\to 0}\Delta\bar{p} = \lim_{\varepsilon\to 0}\hat{f} = 1 + \frac{\beta}{2}, \quad \lim_{\beta\to 0}\Delta\bar{p} = \lim_{\beta\to 0}\hat{f} = 1 - \frac{\varepsilon}{2} \tag{48}$$

The simple expressions given by Eq. (48) reveal that compressibility reduces the volumetric flow-rate throughout the tube (which is expected), as well as the skin friction factor and the pressure difference required to drive the flow, while the pressure-dependent viscosity has the opposite effect, namely it increases the skin friction factor and the required pressure difference (of course the volumetric flow-rate remains constant). Hence, these are competing effects, which for suitable values of the ε, β may counterbalance each other.

In Fig. 4, the volumetric flow-rates at the entrance of the circular tube, $Q(0)$, in both the flow configurations with $\varepsilon = 0.2$ and various values of the aspect ratio are plotted versus β and B. The results have been derived using Eq. (43) and

(a) the exact (numerical) values for λ and for the quantity q_1,

(b) the asymptotic expression λ_{as} given by Eq. (24), and the asymptotic series for q_1, given by the last expression in Eq. (47). In this case, the formula for $Q(0)$ reduces to:

$$Q(0) \approx 1 + \frac{\varepsilon}{\beta}\left\{ 1 + \frac{e^{\beta\lambda_{as}}}{\lambda_{as}}\left(-1 + \frac{B^2}{12} + \frac{B^4}{288} + \frac{B^6}{2880} \right) \right\} \tag{49}$$

For the sake of comparison, the results for the planar configuration are also shown (in this case, $Q(0)$ is given by Eq. (50) in the following subsection). First, it is clear that the asymptotic and exact values for $Q(0)$ are indistinguishable; this indicates that Eq. (50) is an excellent approximation of Eq. (43). Second, it appears that when $Q(0)$ is depicted as a function of β the effect of the aspect ratio a is negligible. Third, the results for the two flow configurations are practically the same (the differences are not visible). Last, and most importantly, the effect of the viscosity-pressure-dependence coefficient β on the volumetric flow-rate at the entrance of the tube is dramatic; recall that for an incompressible fluid, i.e., for $\varepsilon = 0$, $Q(0) = 1$,
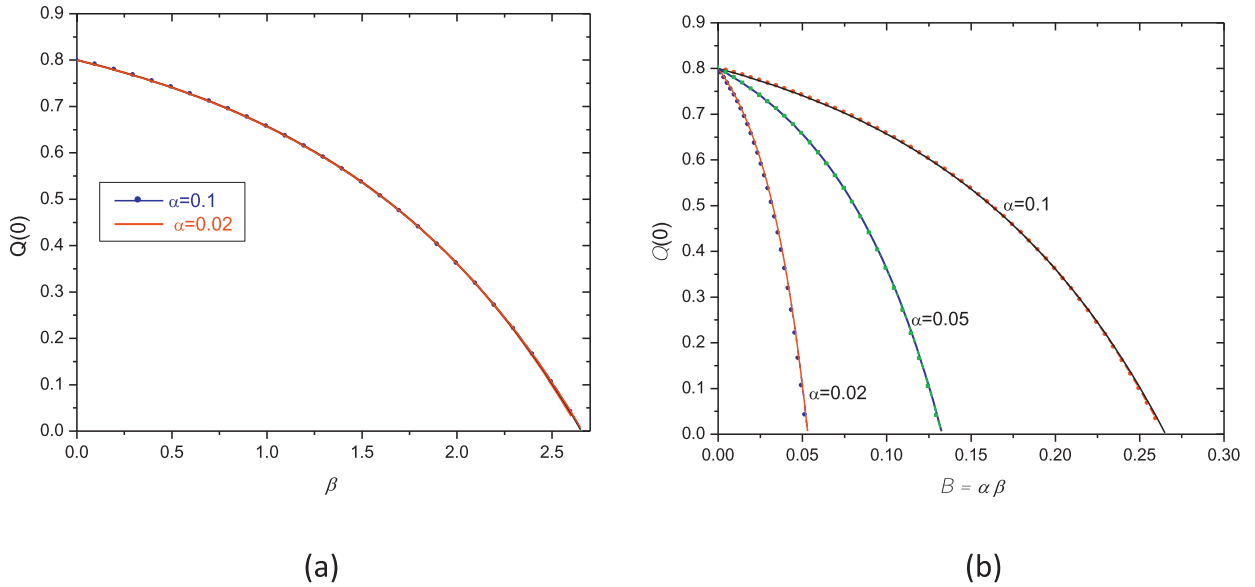
Fig. 4. Volumetric flow rate at the inlet for both the planar (dots) and axisymmetric (solid lines) configurations with $\varepsilon = 0.2$ and various aspect ratios: (a) versus β; (b) versus $B = \alpha \beta$.

while for a compressible fluid with constant viscosity ($\beta = 0$), $Q(0) = 1 - \varepsilon$. In particular, $Q(0)$ decreases monotonically with β resulting in zero flow-rate at $\beta \approx 2.63$. The plot of the volumetric flow-rate at the entrance of the tube/channel versus the modified pressure-dependence coefficient B in Fig. 4b is also very interesting. In this case, the effect of the aspect ratio is clear; as a is increased $Q(0)$ drops sharply and vanishes eventually and thus the analytical solution is valid for lower values of B. For instance, when $a = 0.1$, $Q(0)$ vanishes at a critical value $B_{cr} \approx 0.27$, while for $a = 0.05$ and 0.02, the values of B_{cr} are roughly 0.13 and 0.053, respectively.

Eq. (43) can also provide an upper limit of validity of the analytical solution in terms of the compressibility number. Indeed, the solution has a physical meaning only when the volumetric flow-rate at the entrance of the tube is positive, i.e., $Q(0) > 0$. By solving $Q(0) = 0$ a critical value for ε, ε_{cr}, can be found. Obviously, when $\varepsilon \geq \varepsilon_{cr}$ the solution is not valid. Results for ε_{cr} as a function of the modified coefficient $B \equiv a\beta$ are given in Fig. 5, for both flow configurations and various aspect ratios ($a = 0.1$, 0.01, and 0.001). Note that the results for the two flow configurations are indistinguishable. We observe that ε_{cr} drops fast as B is increased. For example, $\varepsilon_{cr} \approx 10^{-5}$ for a short channel/tube with $a = 0.1$ and $\beta = B/a \approx 10.6$, while for $a = 0.01$ and 0.001 one finds $\beta = B/a \approx 14.1$.

In Fig. 6a, $\hat{f}$ and $\Delta \bar{p}$ for $\varepsilon = 0.2$ and three aspect ratios $a = 0.1$, 0.05, and 0.02 are plotted as functions of $B = a\beta$ (only results for $B < B_{cr}$ are shown). Both quantities increase with B reaching a maximum beyond which they decrease sharply. These maxima are due to the competing effects of compressibility and viscosity pressure-dependence. Note that in incompressible flow $\hat{f}$ and $\Delta \bar{p}$ would increase monotonically with β until solution is lost (Kalogirou et al., 2011). On the other hand, weak compressibility reduces $\hat{f}$ and $\Delta \bar{p}$. Depending on the magnitudes of ε and β, one effect may dominate the other. From Eq. (41), we also see that $\hat{f}$ and $\Delta \bar{p}$ are not identical although their values are very close; some minor differences can be observed only for a short tube ($a = 0.1$) and for high values of the modified dimensionless pressure-viscosity coefficient B. The effect of the aspect ratio becomes less pronounced when plotting the same quantities versus β, which was also the case with the volumetric flow-rate in Fig. 4.

4.2. Planar flow

The expressions for the volumetric flow rate, the average pressure drop, and the Darcy friction factor in the cased of planar flow are as follows:

$$Q(z) = 1 + \frac{\varepsilon}{\beta} \left\{ 1 + \frac{3e^{\lambda\beta(1-z)}}{B^3\lambda^2 \cosh(B\lambda)} \left(2\tan^{-1}(e^{B\lambda}) - \frac{\pi}{2} - \sinh(B\lambda) \right) \right\} \tag{50}$$

$$\Delta \bar{p} = \Delta \bar{p}_0 + \varepsilon \left\{ \frac{a}{3\tanh(B\lambda) - 2B} \left(\frac{\tanh(B\lambda)}{B\lambda\beta} \left[e^{\lambda\beta}(\beta\lambda - 1) + 1 \right] + \frac{e^{\lambda\beta} - 1}{\beta\cosh^2(B\lambda)} \right) \right. $$
$$\left. + \frac{\tanh(B\lambda)}{B\lambda}(1 - e^{\lambda\beta})h(1) + (e^{2\lambda\beta} - 1)\Phi_0 \right\} \tag{51}$$
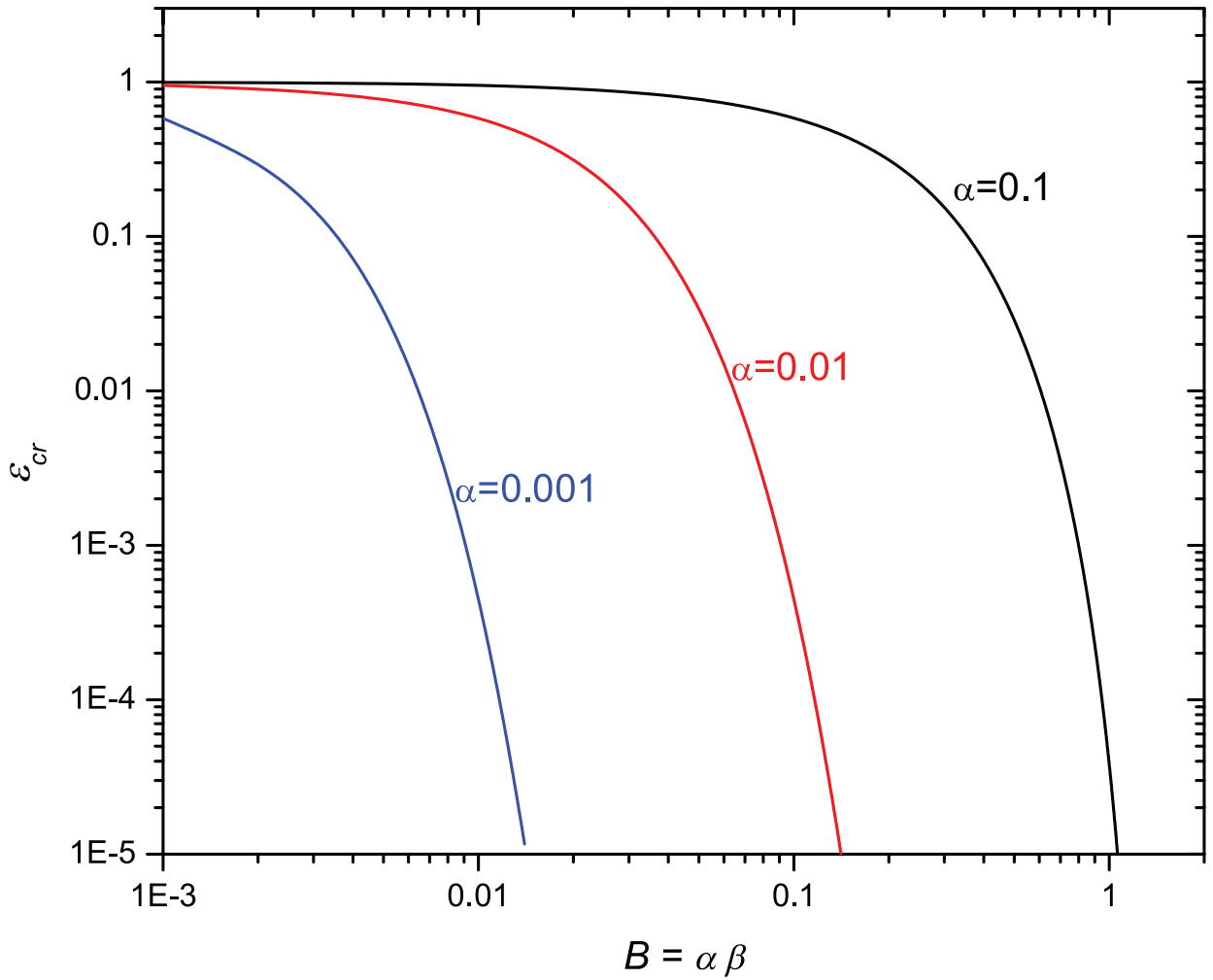
Fig. 5. Critical value of the dimensionless compressibility parameter above which the solution is not valid for both the planar and the axisymmetric flows and various aspect ratios.
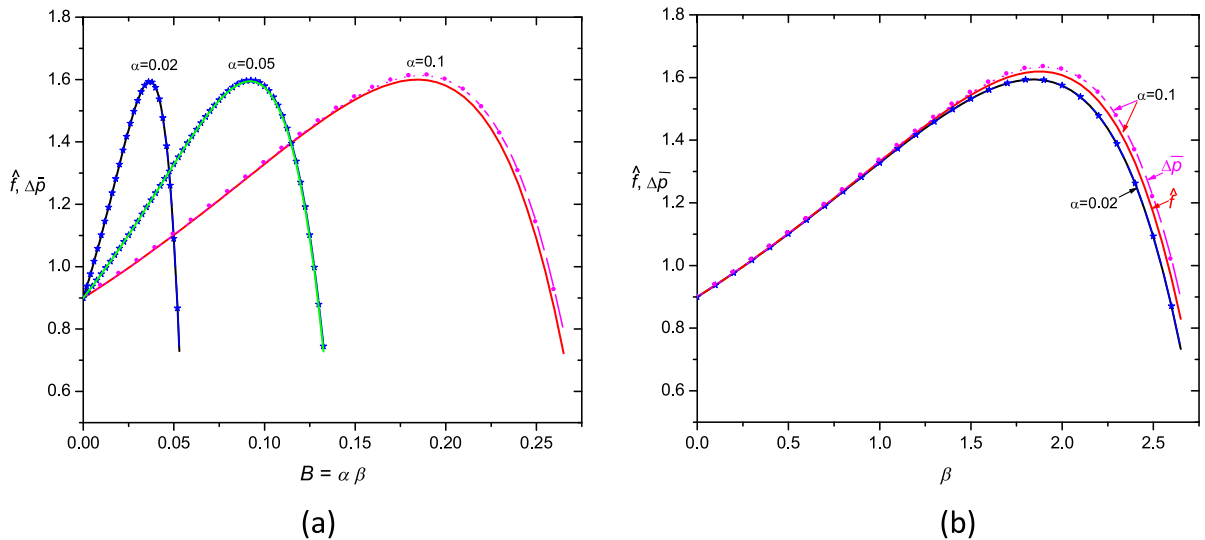

Fig. 6. Average pressure drops $\Delta \bar{p}$ (dashed with symbols) and mean Darcy friction factors $\hat{f}$ (solid lines) in axisymmetric flow with $\varepsilon = 0.2$ and various aspect ratios: (a) versus $B = \alpha \beta$; (b) versus β.
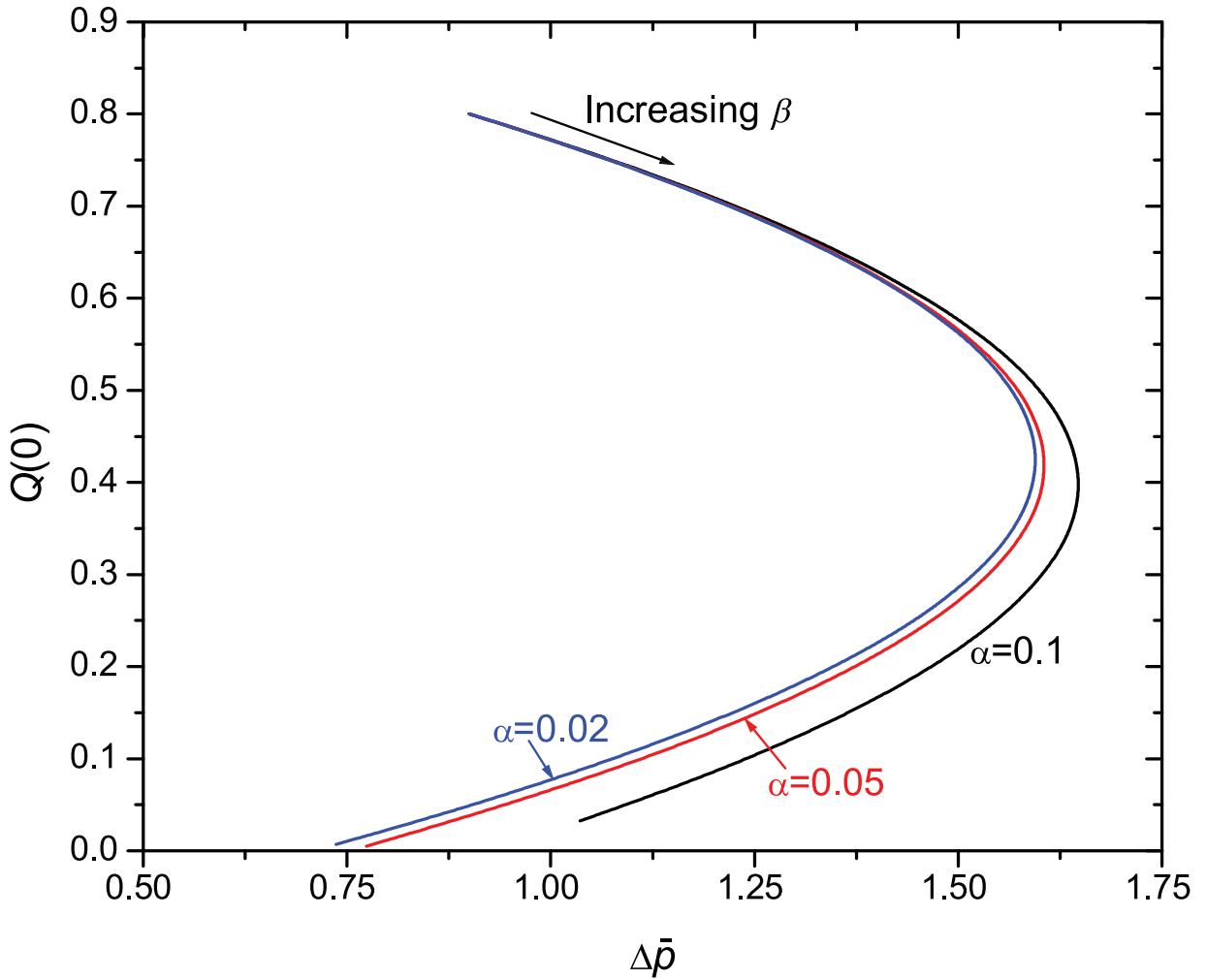
Fig. 7. The volumetric flow rate at the entrance of the channel (planar flow) for $\varepsilon = 0.2$ and various aspect ratios.

$$\hat{f} = \Delta \bar{p}_0 + \varepsilon \left\{ \frac{\tanh(B\lambda)}{2B\lambda\beta^2}(1 - e^{\lambda\beta})\left(1 + \beta^2 h(1) + e^{\lambda\beta}(1 - \beta^2 h(1))\right) + \frac{1 - e^{2\lambda\beta}}{6\beta^2\lambda^2}\hat{u}_{r1}''(1) \right.$$

$$\left. + \frac{\left(1 + e^{\lambda\beta}(\lambda\beta - 1)\right)\sinh(2B\lambda) + 2B\lambda(e^{\lambda\beta} - 1)}{2\lambda\beta^2\cosh^2(B\lambda)[3\tanh(B\lambda) - 2B]} \right\} \tag{52}$$

In Eq. (51), Φ_0 is given as:

$$\Phi_0 \equiv -\frac{\cosh^2(B\lambda)}{3(\lambda\beta)^2}\hat{u}_{r1}''(1) + \frac{\tanh(B\lambda)}{4B\lambda\beta^2}\left(\frac{1}{3} - \frac{3\cosh(2B\lambda)}{2}\right) + \frac{1}{6\cosh^2(B\lambda)}\left(\frac{7a^2\lambda}{3} - \frac{17}{4\beta^2}\right)$$

$$+ \frac{2a^2B\lambda}{3\cosh(B\lambda)}\int_0^1 (5 + 6\cosh(2B\lambda r))\sinh(B\lambda r)\hat{u}_{r1}(r)dr \tag{53}$$

Also, $h(1)$ is found by evaluating Eq. (36) at $r = 1$, $\hat{u}_{r1}(r)$ and $\hat{u}_{r1}''(1)$ are calculated from Eq. (35), while the integral which appears in Eq. (53) is approximated very accurately by:

$$\int_0^1 (5 + 6\cosh(2B\lambda r))\sinh(B\lambda r)\hat{u}_{r1}(r)dr \approx -\frac{121}{525}B^3 - \frac{8789}{47250}B^5 - \frac{3559}{27720}B^7 \tag{54}$$

The volumetric flow-rates at the entrance of the channel for three values of the aspect ratio are shown in Fig. 7 as functions of the average pressure drop. Each curve has been constructed by fixing a and ε, then varying β from zero up to the value at which $Q(0)$ becomes zero, and calculating $Q(0)$ from Eq. (50) with $z = 0$, and $\Delta\bar{p}$ from Eq. (51). Note that different

values of β correspond to different fluids flowing in channels with the same dimensions. These flow curves give information on the pressure difference required to drive the flow and the resulting volumetric flow-rate at the inlet. Interestingly, $\Delta\bar{p}$ increases while $Q(0)$ decreases with β, which is a compressibility effect. However, at a critical value of β a turning point appears beyond which $\Delta\bar{p}$ and $Q(0)$ are decreasing. As a result, for a given value of $\Delta\bar{p}$, two values of $Q(0)$ are possible, the lower of which corresponds to a fluid with a stronger viscosity pressure-dependence (i.e., with a higher value of β).

5. Conclusions

New asymptotic solutions for the steady, planar and axisymmetric, Poiseuille flows of weakly compressible Newtonian fluids with viscosity and mass density that depend linearly on the pressure have been obtained. All the primary flow variables are perturbed in terms of the dimensionless compressibility number ε, and the solution is found up to the first order in ε. The main features of the derived solutions are the following:

(a) All the primary flow variables (velocity, pressure, and viscous stresses) are fully two-dimensional
(b) The wall normal velocity is generated due to the combined effect of compressibility and viscosity pressure-dependence.
(c) The average pressure drop, $\Delta\bar{p}$, required to drive the flow increases with viscosity pressure-dependence and decreases with compressibility.
(d) The behaviour of the mean Darcy friction factor, $\hat{f}$, is similar to that of $\Delta\bar{p}$. However, $\hat{f}$ deviates slightly from $\Delta\bar{p}$ due to the compressibility which generates the extra-stress $\Delta\bar{\tau}_{zz}$.
(e) A dramatic reduction of the volumetric flow at the entrance of the tube/channel is predicted as the dimensionless viscosity pressure-dependence coefficient β is increased.
(f) For a given value of $\Delta\bar{p}$, two volumetric flow-rates at the inlet of the channel/tube are possible the higher of which corresponds to a fluid with a lower β.

The solutions derived here may be useful for the design and control of fluid transport in channels and tubes and other processes involving high pressures at which compressibility and viscosity pressure-dependence effects are important. They may also be used to study various heat transfer problems which are of significance in a variety of practical and industrial applications.

Acknowledgments

Appendix

Double perturbation expansions

The solutions derived in this paper can be expanded as power series in β resulting in double perturbation series for all the flow variables. Assuming that β and ε are of similar magnitude, i.e. $\beta \approx \varepsilon$, and keeping terms of order 1, ε, β, $\varepsilon\beta$ and β^2 suitable double perturbation expansions are derived. In both geometrical flow configurations, the radial velocity component is zero (recall that $u_r = O(\varepsilon\beta^2 a^2)$). The expressions for the other variables follow.

Axisymmetric flow

$$u_z \approx 2(1-r^2)\left\{1 + \frac{(a\beta)^2}{48}(1-3r^2) - \varepsilon(1-z) + \varepsilon\beta\left(\frac{a^2(11+3r^2)}{72} - \frac{(1-z)^2}{2}\right)\right\}$$

$$p \approx (1-z) + \beta\left(\frac{(1-z)^2}{2} - \frac{a^2(1-r^2)}{4}\right) + \beta^2(1-z)\left(\frac{(1-z)^2}{6} - \frac{a^2(2-3r^2)}{12}\right)$$

$$+ \varepsilon\left[-\frac{(1-z)^2}{2} + \frac{a^2(1-r^2)}{12} + \beta(1-z)\left(-\frac{2(1-z)^2}{3} + \frac{a^2(31-24r^2)}{36}\right)\right]$$

$$Q(z) \approx 1 - \varepsilon(1-z) + \varepsilon\beta\left(-\frac{(1-z)^2}{2} + \frac{a^2}{6}\right)$$

$$\Delta\bar{p} \approx 1 + \frac{\beta}{2} + \beta^2\left(\frac{1}{6} - \frac{a^2}{24}\right) - \frac{\varepsilon}{2} + \varepsilon\beta\left(-\frac{2}{3} + \frac{19a^2}{36}\right)$$

$$\hat{f} \approx 1 + \frac{\beta}{2} + \beta^2\left(\frac{1}{6} - \frac{a^2}{24}\right) - \frac{\varepsilon}{2} + \varepsilon\beta\left(-\frac{2}{3} + \frac{7a^2}{36}\right)$$

The above expressions are identical to those derived by Poyiadji et al. (2015).

Planar flow

$$u_z \approx \frac{3}{2}(1-r^2)\left\{1 + \frac{(a\beta)^2}{30}(1-5r^2) + \varepsilon\left[-(1-z) + \beta\left(-\frac{(1-z)^2}{2} + \frac{a^2(23+5r^2)}{60}\right)\right]\right\}$$

$$p \approx (1-z) + \frac{\beta}{2}\left((1-z)^2 - a^2(1-r^2)\right) + \beta^2(1-z)\left(\frac{(1-z)^2}{6} + \frac{a^2(-3+5r^2)}{10}\right)$$

$$+ \varepsilon\left[-\frac{(1-z)^2}{2} + \frac{a^2(1-r^2)}{6} + \beta(1-z)\left(-\frac{2}{3}(1-z)^2 + \frac{a^2(27-20r^2)}{15}\right)\right]$$

$$Q(z) \approx 1 - \varepsilon(1-z) + \varepsilon\beta\left(-\frac{(1-z)^2}{2} + \frac{2a^2}{5}\right)$$

$$\Delta\bar{p} \approx 1 + \frac{\beta}{2} + \beta^2\left(\frac{1}{6} - \frac{2a^2}{15}\right) - \frac{\varepsilon}{2} + \varepsilon\beta\left(-\frac{2}{3} + \frac{61a^2}{45}\right)$$

$$\hat{f} \approx 1 + \frac{\beta}{2} + \beta^2\left(\frac{1}{6} - \frac{2a^2}{15}\right) - \frac{\varepsilon}{2} + \varepsilon\beta\left(-\frac{2}{3} + \frac{7a^2}{15}\right)$$

Again, the above expressions are the same as those found by Poyiadji et al. (2015).

Auxiliary functions

The auxiliary function $h = h(r)$ which appears in the analytical solution (Eqs. (26)–(27) for the axisymmetric case, and Eq. (33) for the planar case) is given in terms of $\hat{p}_0$ and $\hat{u}_{r1}$:

$$h(r) = \frac{a^2\hat{p}_0}{(3+5\xi)\left(\hat{p}_0'^2 - (a\lambda\beta\hat{p}_0)^2\right)}\left\{\begin{array}{l} \hat{u}_{r1}''' + \left(\frac{2\xi}{r} + \frac{\hat{p}_0'}{\hat{p}_0}\right)\hat{u}_{r1}'' + \left(3(a\lambda\beta)^2 - \frac{\xi}{r^2} + \frac{\xi\hat{p}_0'}{r\hat{p}_0} - 2\frac{\hat{p}_0'^2}{\hat{p}_0^2}\right)\hat{u}_{r1}' \\[2mm] + \left(\frac{\xi}{r^3}\left(1 - \frac{r\hat{p}_0'}{\hat{p}_0} + 3(a\lambda\beta r)^2\right) - 3(a\lambda\beta)^2\frac{\hat{p}_0'}{\hat{p}_0}\right)\hat{u}_{r1} \\[2mm] + \frac{3+5\xi}{3}\left[\lambda^2\hat{p}_0^2(3 + 11\ln(\hat{p}_0)) + \frac{5\hat{p}_0'^2(2 + \ln(\hat{p}_0))}{(a\beta)^2\hat{p}_0}\right] \end{array}\right\}$$

The full ordinary differential equation (ODE) for $\hat{u}_{r1}$ is:

$$\hat{u}_{r1}^{(4)}(r) + g_3(r)\hat{u}_{r1}^{(3)}(r) + g_2(r)\hat{u}_{r1}''(r) + g_1(r)\hat{u}_{r1}'(r) + g_0(r)\hat{u}_{r1}(r) = g(r) \tag{A1}$$

where

$$g(r) = \frac{(3+5\xi)\lambda^2\hat{p}_0'}{c^2\hat{p}_0^2 - \hat{p}_0'^2}\left\{-c^2\hat{p}_0^2(11+10\ln(\hat{p}_0)) + \frac{4\hat{p}_0'^2(6+7\ln(\hat{p}_0))}{3} + \frac{\hat{p}_0'^4(9+2\ln(\hat{p}_0))}{3c^2\hat{p}_0^2} + \frac{2\xi\hat{p}_0\hat{p}_0'(13+16\ln(\hat{p}_0))}{3r}\right\}$$

$$g_0(r) = -c^2\left(c^2 + \frac{2\hat{p}_0'^2}{\hat{p}_0^2}\right) + \frac{\xi}{r^3(c^2\hat{p}_0^2 - \hat{p}_0'^2)}\left\{-\frac{c^2(3+4c^2r^2)\hat{p}_0^2}{r} + 2c^2(2+3c^2r^2)\hat{p}_0\hat{p}_0' + \frac{(1-2c^2r^2)\hat{p}_0'^2}{r} - \frac{2\hat{p}_0'^3}{\hat{p}_0}\right\}$$

$$g_1(r) = -\frac{2c^2\hat{p}_0'}{\hat{p}_0} + \frac{\xi}{r^2(c^2\hat{p}_0^2 - \hat{p}_0'^2)}\left\{\frac{c^2(3+4c^2r^2)\hat{p}_0^2}{r} - 4c^2\hat{p}_0\hat{p}_0' - \frac{(1+6c^2r^2)\hat{p}_0'^2}{r} + \frac{2\hat{p}_0'^3}{\hat{p}_0}\right\}$$

$$g_2(r) = 4c^2 - \frac{2\hat{p}_0'^2}{\hat{p}_0^2} + \frac{\xi}{r}\left\{\frac{1}{r} + \frac{4\hat{p}_0'}{\hat{p}_0} - \frac{2c^2\hat{p}_0(2\hat{p}_0 + r\hat{p}_0')}{r(c^2\hat{p}_0^2 - \hat{p}_0'^2)}\right\}$$

$$g_3(r) = 2\frac{\hat{p}_0'}{\hat{p}_0} + \frac{2\xi}{r}\left\{2 - \frac{c^2\hat{p}_0^2}{c^2\hat{p}_0^2 - \hat{p}_0'^2}\right\}$$

and $c \equiv B\lambda$ has been used for convenience. Eq. (A1) is a fourth-order, non-homogeneous, ordinary differential equation with non-constant coefficients, accompanied by the homogeneous boundary conditions:

$$\hat{u}_{r1}(0) = \hat{u}_{r1}(1) = \hat{u}_{r1}'(1) = 0, \text{ and}$$
$$\hat{u}_{r1}''(0) = 0 \quad \text{for } \xi = 0$$
$$\lim_{r\to 0}\left(\frac{\hat{u}_{r1}'(r)}{r} - \frac{\hat{u}_{r1}(r)}{r^2} + \hat{u}_{r1}''(r)\right) = 0 \quad \text{for } \xi = 1$$
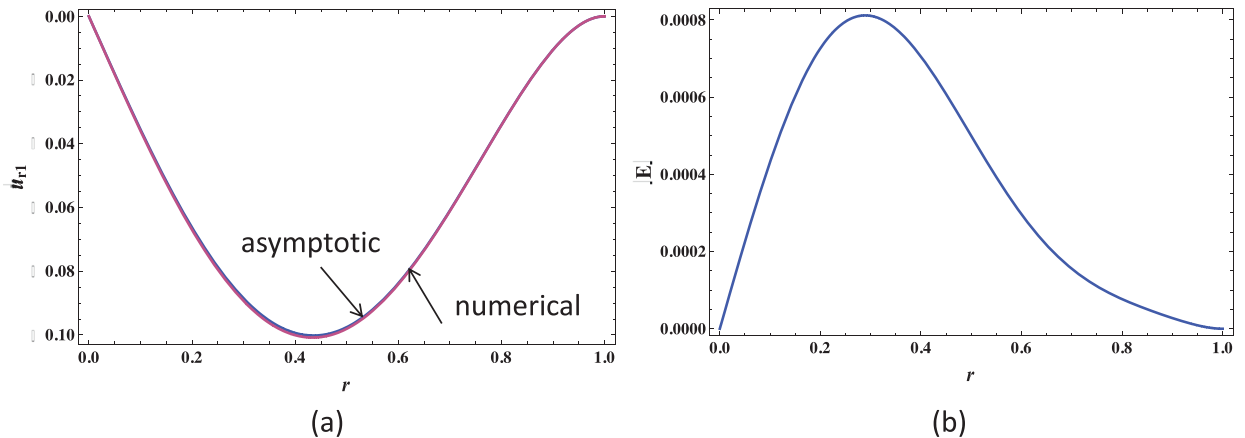
Fig. 8. (a) Numerical and asymptotic solutions for $\hat{u}_{r1}$ in planar flow with $\alpha = 0.1$ and $\beta = 10$ (a rather extreme value to exaggerate the differences); (b) The absolute error of the asymptotic solution.

However, given the complexity of functions $g, g_0, g_1, g_2,$ and g_3, it cannot be solved analytically; it can be solved numerically though for any value of β, or asymptotically for small values of β. Both numerical and asymptotic solutions (see Section 3) have been calculated for $\hat{u}_{r1} = \hat{u}_{r1}(r)$ and $h = h(r)$. In order to determine the accuracy and validity of the asymptotic solution, Eq. (A1) has been solved numerically for different aspect ratios, a, and pressure-dependent coefficients, β. In general, the asymptotic solution for $\hat{u}_{r1}$ is an excellent approximation of the exact solution up to $B \approx 1$. Fig. 8 shows numerical results for $\hat{u}_{r1}$ in the case of planar flow. A short channel with $a = 0.1$ and a fluid with very large pressure-viscosity coefficient, $\beta = 10$, have been chosen (resulting to $B=1$) so that the radial velocity is exaggerated in order to test the accuracy of the asymptotic solution. It is seen that $\hat{u}_{r1}$, which vanishes at $r = 0$ and $r = 1$ due to the symmetry and no-penetration conditions respectively, is always negative and passes through a minimum at $r \approx 0.75$. The absolute error between the asymptotic and numerical solution, $|E|$, is presented as a function of the radial distance r in Fig. 8b. It is seen that $|E|$ exhibits similar behavior with $\hat{u}_{r1}$. Numerical results for $B < 1$ confirm that $|E|$ drops close to machine accuracy, clearly indicating the robustness and validity of the asymptotic solution for $\hat{u}_{r1}$.

References

Barus, C. (1891). Note on dependence of viscosity on pressure and temperature. *Proceedings of the American Academy, 27*, 13–19.
Barus, C. (1893). Isothermals, isopiestics and isometrics relative to viscosity. American Journal.of Science., *45*, 87–96.
Bollada, P. C., & Phillips, T. N. (2012). On the mathematical modelling of a compressible viscoelastic fluid. *Archive for Rational Mechanical. Analysis., 205*, 1–26.
Dealy, J. M., & Wang, J. (2013). *Melt rheology and its applications in the plastics industry* (2nd Ed.). Dordrecht: Springer.
Denn, M. M. (2008). *Polymer melt processing*. Cambridge: Cambridge University Press.
Fusi, L., Farina, A., & Rosso, F. (2015). Mathematical models for fluids with pressure-dependent viscosity in porous media. *International Journal. of Engineering. Science, 87*, 110–118.
Georgiou, G. C. (2003). The time-dependent, compressible Poiseuille and extrudate-swell flows of a Carreau fluid with slip at the wall. Journal. of Non-Newtonian Fluid Mechanics., *109*, 93–114.
Gustafsson, T., Rajagopal, K. R., Stenberg, R., & Videman, J. (2015). Nonlinear Reynolds equation for hydrodynamic lubrication. *Applications in Mathematics Modelling, 39*, 5299–5309.
Hamrock, B. J., Schmid, S. R., & Jaconson, B. O. (2004). *Fundamentals of fluid film lubrication*. New York: Marcel Dekker.
Housiadas, K. D. (2015). Internal viscoelastic flows for fluids with exponential type pressure-dependent viscosity and relaxation time. *Journal of Rheology, 59*(3), 769–791.
Housiadas, K. D., Georgiou, G. C., & Tanner, R. I. (2015). A note on the unbounded creeping flow past a sphere for Newtonian fluids with pressure-dependent viscosity. *International Journal of Engineering Science, 86*, 1–9.
Huilgol, R. R., & You, Z. (2006). On the importance of the pressure dependence of viscosity in steady non-isothermal shearing flows of compressible and incompressible fluids and in the isothermal fountain flow. *Journal of Non-Newtonian Fluid Mechanics, 136*, 106–117.
Ionescu, I. R., Mangeney, A., Bouchut, F., & Roche, O. (2015). Viscoplastic modeling of granular column collapse with pressure-dependent rheology. *Journal of Non-Newtonian Fluid Mechanics, 219*, 1–18.
Kadjik, S. E., & van Den Brule, B. H. A. A. (1994). On the pressure dependency of the viscosity of molten polymers. *Polymer Engineering and Science, 34*, 1535–1546.
Kalogirou, A., Poyiadji, S., & Georgiou, G. C. (2011). Incompressible Poiseuille flows of Newtonian liquids with a pressure-dependent viscosity. *Journal of Non-Newtonian Fluid Mechanics, 166*, 413–419.
Kottke, P. A., Bair, S. S., & Winer, W. O. (2003). The measurement of viscosity of liquids under tension,. *Transactions of the* ASME, *125*, 260–266.
Li, C., Jiang, F., Wu, L., Yuan, X., & Li, X. (2015). Determination of the pressure dependence of the shear viscosity of polymer melts using a capillary rheometer with an attached counter pressure chamber,. *Journal of* Macromolecular Science, Part B: Physics, *54*, 1029–1041.
Málek, J., & Rajagopal, K. R. (2007). Mathematical properties of the solutions to the equations governing the flow of fluids with pressure and shear rate dependent viscosities. In S. Friedlander, & S. Serre (Eds.). In *Handbook of mathematical fluid dynamics. handbook of mathematical fluid dynamics: 4* (pp. 407–444). Amsterdam: Elsevier.
Martinez-Boza, F. J., Martin-Alfonso, M. J., Callegos, C., & Fernández, M. (2011). High-pressure behavior of intermediate fuel oils. *Energy Fuels, 25*, 5138–5144.
Prusa, V. (2010). Revisiting Stokes first and second problems for fluids with pressure-dependent viscosities. *International Journal of Engineering Science, 48*, 2054–2065.

Poyiadji, S., Housiadas, K. D., Kaouri, K., & Georgiou, G. C. (2015). Asymptotic solutions of weakly compressible Newtonian Poiseuille flows with pressure-dependent viscosity. *European Journal of Mechanics B-Fluids, 49*, 217–225.

Rajagopal, K. R. (2006). On implicit constitutive theories for fluids. *Journal of Fluid Mechanics, 550*, 243–249.

Rajagopal, K. R., Saccomandi, G., & Vergori, L. (2012). Flow of fluids with pressure- and shear-dependent viscosity down an inclined plane. *Journal of Fluid Mechanics, 706*, 173–189.

Rehor, M., & Prusa, V. (2016). Squeeze flow of a piezoviscous fluid. *Application in Maths Computing, 274*, 414–429.

Renardy, M. (2003). Parallel shear flows of fluids with a pressure-dependent viscosity. *Journal of Non-Newtonian Fluid Mechanics, 114*, 229–236.

Schaschke, C., Fletcher, I., & Glen, N. (2013). Density and viscosity measurement of diesel fuels at combined high pressure and elevated temperature. *Processes, 1*, 30–48.

Schoof, C. (2007). Pressure-dependent viscosity and interfacial instability in coupled ice sediment flow,. *Journal of* Fluid Mech*anics, 570*, 227–252.

Silber-Li, Z., Cui, H., Tan, Y., & Tabeling, P. (2006). Flow characteristics of liquid with pressure-dependent viscosities in microtubes. *Acta Mechanica Sinica, 22*, 17–21.

Stemmer, K., Harder, H., & Hansen, U. (2006). A new method to simulate convection with strong temperature- and pressure-dependent viscosity in a spherical shell: Applications to the Earth's mantle. *Physics Earth Planet. Interiors, 157*, 223–249.

Taliadorou, E., Georgiou, G., & Mitsoulis, E. (2008). Numerical simulation of the extrusion of strongly compressible Newtonian liquids. *Rheologica Acta, 47*, 49–62.

Taliadorou, E., Neophytou, M., & Georgiou, G. C. (2009). Perturbation solutions of Poiseuille flows of weakly compressible Newtonian liquids. *Journal of Non-Newtonian Fluid Mechanics, 158*, 162–169.

Tanner, R. I. (2000). *Engineering rheology*. Oxford: Oxford University Press.

Vasudevaiah, M., & Rajagopal, K. (2005). On fully developed flows of fluids with a pressure dependent viscosity in a pipe. *Applications of Mathematics, 50*, 341–353.

Venerus, D. C. (2006). Laminar capillary flow of compressible viscous fluids. *Journal of Fluid Mechanics, 555*, 59–80.

Venerus, D. C., & Bugajsky, D. J. (2010). Laminar flow in a channel. *Physics of Fluids, 22*, 046101.

Venner, C., & Lubrecht, A. A. (2000). *Multilevel methods in lubrication*. Oxford: Elsevier Science B.V.

Vinay, G., Wachs, A., & Frigaard, I. (2006). Numerical simulation of weakly compressible Bingham flows: The restart of pipeline flows of waxy crude oils. *J. Non-Newtonian Fluid Mech., 136*, 93–100.

van den Berg, H. R., Seldam, C. A., & van der Gulik, P. S. (1993). Compressible laminar flow in a capillary. *Journal of Fluid Mechanics, 246*, 1–20.

Srinivasan, S., & Rajagopal, K. R. (2009). Study of a variant of Stokes' first and second problems for fluids with pressure dependent viscosities. *International Journal of Engineering Science, 47*, 1357–1366.